# A kinetic study of the influence of humic acids on the oxidation of As(III) by acid birnessite

David Nielsen-Franco [1], Matthew Ginder-Vogel* [1,2]

1. Environmental Chemistry and Technology program, University of Wisconsin-Madison, USA
2. Department of Civil and Environmental Engineering, University of Wisconsin-Madison, USA

**Corresponding author:**

**Matthew Ginder-Vogel –** Department of Civil and Environmental Engineering, University of Wisconsin-Madison, Madison, Wisconsin, United States; orcid.org/0000-0001-9183-1931; Email: mgindervogel@wisc.edu

**ABSTRACT:** Dissolved arsenic (As) in natural environments is controlled by sorption onto metal oxide surfaces; its speciation is principally influenced by biogenic manganese oxides and natural organic matter (NOM). Manganese (III/IV) oxides are strong oxidants that are ubiquitous in soils and sediments; and humic acids (HA) are typical substances found in the dissolved fraction of NOM. However, the mechanism of As(III) oxidation by $MnO_2$ in the presence of NOM remains poorly understood. Here, we investigate how HA, impact the oxidation of As(III) by a synthetic manganese oxide, i.e., acid birnessite ($MnO_2$). We find that the reaction kinetics of As with HA and $MnO_2$ are controlled by formation of surface complexes. The main observed effect is a decrease of the overall oxidation rate in the presence of HA. In addition, pre-exposure of $MnO_2$ to HA for 24 hours further decreases the reaction rate, which is attributed to the occupation of $MnO_2$ surface active sites; thus, causing surface passivation. Our results demonstrate that HA influence the reaction mechanism of As(III) oxidation by $MnO_2$ via sorption onto active surface sites and the formation of aqueous complexes.

**KEYWORDS:** *arsenic, kinetics, mechanisms, Langmuir-Hinshelwood, manganese oxides*

**Synopsis:** The mechanism of arsenite oxidation by acid birnessite is influenced by the presence of humic acids in aqueous systems.

## INTRODUCTION

Arsenic (As) is a ubiquitous and toxic element present in drinking water sources around the world.[1–4] Geogenic As contamination of groundwater is a worldwide concern, the most affected regions are located in South America and Southeast Asia.[3,4,9] The World Health Organization (WHO) has set a provisional guideline of 10 $\mu g \cdot L^{-1}$ As in drinking water, given its classification as a carcinogen and mutagen; higher levels are associated with adverse health effects.[3,6,7] In As-contaminated soils like mine tailings, flooded paddies, or acid mine drainage, speciation of As is regulated by simultaneous reactions occurring on mineral surfaces (iron, aluminum, and manganese oxides); mainly precipitation, oxidation/reduction, and adsorption/desorption.[8–10] As mobility in the environment is primarily controlled by adsorption on Mn and Fe oxides.[9,11–17] The most abundant forms of dissolved inorganic As in common environmental conditions are As(III), present as $H_3AsO_3$; and As(V), present as $H_2AsO_4^-$ and $HAsO_4^{2-}$, at circumneutral pH. As(III) is generally considered to be more toxic and mobile than As(V), given that the latter tends to strongly adsorb to positively charged mineral surfaces.[15]

Natural organic matter (NOM) is ubiquitous in environmentally relevant systems, existing as a complex mixture of organic material that impacts the reactivity, speciation, solubility, and mobility of oxyanions, metal cations, and mineral surfaces.[13,18] NOM increases As solubility via the formation of NOM-As complexes.[8,19–21] Dissolved organic matter (DOM), a subset of NOM, is an aqueous heterogeneous mixture of macromolecules of which about 80% consist of humic substances.[13,22] Humic acids (HA), a fraction of humic substances, possess diverse functional groups with varying pKa values,[12,23] but the average charge on HA is generally neutral to negative at circumneutral pH. Carboxyl, phenolic, and hydroxyl functional groups are often involved in mineral surface interaction and cation complexation;[13] along with the amino groups, these moieties

are predominantly involved in the formation of As-humic acid complexes (AsHA).[24–26] The presence of HA strongly influences As mobility mainly via competitive adsorption and complexation.[8,12,13,23] In contaminated soils, HA significantly increase the release of As by forming aqueous complexes.[8]

In addition to complexation with organic matter, As speciation and solubility is impacted by pH, redox conditions, the presence of mineral surfaces and other ligands.[13,27] Mono- and di-methylated As species, resulting from metabolic activities, are less common in environmental settings than inorganic As(III) and As(V).[13,28,29] However, complexation with NOM plays a vital role in As mobility; dissolution of naturally-adsorbed As on soils and sediments is promoted by its complexation with HA, which forms stronger As(III) complexes than As(V).[8,13,27,30,31] The presence of HA increases the release of As from soils and sediments; under alkaline conditions via competition for sorption sites and complexation.[8,12,23,27,32] Under acidic conditions, adsorbed HA results in As sorption onto soils and sediments via tertiary sorption via metal cation bridges.[27]

Layered Mn(III/IV) oxides are important, environmentally relevant oxidants of As(III).[33–35] The overall reaction mechanism involves As(III) oxidation producing Mn(II) and As(V); the latter partially adsorbs to the surface edges, while the former adsorbs to vacant sites often reacting with Mn(IV) to form Mn(III).[1,35] The presence of NOM often limits As oxidation by impacting its interaction with the mineral surface.[12,13] For instance, the adsorptive properties of mineral surfaces are altered by the formation of a NOM coating.[13,36] Oxidation of NOM by Mn oxides occurs in oxic and suboxic conditions, competing against other contaminants in anthropogenic systems, including As.[37,38] Therefore, a more detailed understanding of the complex interactions taking place in is required to explain As speciation and its depletion rate in the presence of NOM.

Empirical and process-based kinetic models have been proposed to describe the reaction between As(III) and Mn oxides; nevertheless, these simplified models lack a molecular base for

their reaction mechanism.[1,39–41] Pseudo-first or second order kinetics are generally used to describe this reaction; however, given its multistep nature, the rate expression is inherently more complex than these approximations.[1,14,41–45] Given that as As(III) oxidation progresses, $MnO_2$ surface becomes passivated by sorption of As(V) and Mn(II) followed by Mn(III) formation via conproportionation, effectively decreasing surface reactivity; even though oxidation is initially rapid, the reaction slows down considerably.[34,35] This causes the global reaction to have two different kinetic regimes, and is thus improperly described by pure kinetic rate models; rendering the first or second order linearization approach useless.[1]

For surface electron transfer to occur, adsorption on the mineral surface must take place; As(III) oxidation rate is controlled by its adsorption on $Mn^{III/IV}O_2$ edge sites, with an overall second order rate.[41,45] Adsorption of As(III) involves inner-sphere surface complexation which results in the formation of adsorbed surface precursor complexes ($As{\equiv}MnO_2$).[40,45] Nonetheless, previous studies barely considered simultaneous oxidation and reversible adsorption of As(III).[39,46,47] Therefore, Langmuir-Hinshelwood (LH) kinetics are the best approach to model the reaction mechanism, since all species react when chemisorbed on a surface.[1,33,48–53] Feng et al. (2018) develop a LH-type model which describes simultaneous As(III) adsorption/desorption/oxidation, and adsorption/desorption of As(V) on δ-$MnO_2$; their model accurately describes coupled As kinetics on a stir-flow reactor setup and successfully accounts for surface passivation.[54] While their model provides a useful quantitative tool to assess As(III) oxidation on Mn oxides, it is mostly limited to kinetics at initial stages of the reaction and only accounts for two components, $As^{III/V}$ and δ-$MnO_2$. Hence, a more robust approach is necessary to describe more complicated systems, containing HA, throughout the entire reaction.

This study examines As(III) oxidation with $MnO_2$ in the presence of HA employing four different systems. To optimally determine the most suitable model and its parameters, each system

is fit with a different model using non-linear curve fitting (NLCF).[55] Additionally, we investigate the effects of HA on the heterogeneous oxidation of As(III) by comparing the calculated rate constants. Transformation of acid birnessite is also studied by assessing the formation and stability of Mn(III) in the presence of HA. Our results demonstrate that (1) models based on LH kinetics accurately describe the reaction between As, $MnO_2$, and HA; (2) the presence of HA decreases As(III) oxidation rate; and (3) $MnO_2$ release Mn(III) as the reaction progresses and is stabilized by HA in aqueous solution.

## MATERIALS AND METHODS

### Materials

Commercially available chemicals were used as received; for more information see Supporting Information (SI) section S1.1. As(III) and As(V) stock solutions were prepared in an aqueous solution containing 1% or 10% trace metal grade HCl and stored at 4 °C.

**Synthesis and characterization of acid-birnessite.** We synthesized acid-birnessite ($MnO_2$) using a modified procedure which involved the reduction of $KMnO_4$ with concentrated HCl.[37,56,57] Briefly, on a hot plate, 300 mL of a 0.66 mol·L$^{-1}$ $KMnO_4$ solution were boiled and vigorously stirred at 350 rpm. Followed by a dropwise addition of 45 mL of a 6 mol·L$^{-1}$ HCl solution at a rate of 0.8 mL·min$^{-1}$. Once all HCl was added, the solution was stirred overnight at 60 °C for 18 hours. The solid was separated by centrifugation (4000 rpm for 10 minutes) and washed with Milli-Q (18.2 MΩ cm) water, this process was repeated at least 5 times. The supernatant was decanted and the acid birnessite slurry was then dried in an oven at 60 °C for 24 hours and stored in a desiccator under vacuum at room temperature (22 ± 1 °C). X-Ray diffraction analyses were conducted in a Rigaku Rapid II diffractometer with a Mo X-ray source (λ=0.71 Å).

The diffraction pattern was fit using a crystal structure database (JADE, PDF 4+), confirming the presence of only birnessite in the powder sample (Figure S1.1 in SI) with characteristic X-ray diffraction peaks at 1.4 A˚ and 2.4 A˚, indicating a hexagonal layer structure. Two additional peaks at 3.6 A˚ and 7.2 A˚ indicated a randomly-stacked layer structure.[14,58] The morphology of the solid was probed by scanning electron microscopy (SEM) using a Zeiss Gemini SEM 450 equipped with a Schottky type field emission gun. SEM scans show that acid birnessite has a typical morphology of a hexagonal birnessite, consisting of two-dimensional disk-shaped nanoplates within three-dimensional microspheres aggregated as particle clusters (Figure S1.2 in SI).[59,60] The point of zero charge (PZC) was determined to be 2.3 using the pH drift method.[61,62] Briefly, 0.028 g of acid birnessite were placed inside a 250 mL solution containing 10 $mmol \cdot L^{-1}$ NaCl. Four separate reactors were used, each adjusted to a different pH (1, 2, 3 or 4) leaving minimal headspace and stirred at 600 rpm. After 24 hours the pH was measured to quantify drift 'ΔpH' (Figure S1.3 in SI).[1] The specific surface area was determined to be 26.15 $m^2 \cdot g^{-1}$ by nitrogen adsorption using a Brunauer-Emmett-Teller (BET) method in a Quantachrome NovaTouch LX BET surface characteristic analyzer (Anton Paar).

**Quantification of Mn(III).** Two hundred microliters of filtered sample were added to a 50 $mmol \cdot L^{-1}$ sodium pyrophosphate (NaPP) solution at pH=8.0, along with a 10 $mmol \cdot L^{-1}$ Mn(III)-Pyrophosphate (Mn-PP) stock solution. The solutions were thoroughly mixed and reacted in the dark for 30 minutes to ensure quantitative formation of the Mn-PP complex.[63,64] Quantification of Mn(III) in solution was performed according to Kostka et al. (1995),[65,66] using a Horiba Aqualog fluorimeter (S2 in SI). Mn(III) was determined at 2, 4, and 24 hours throughout the batch reactions. To calculate Mn(III) concentration, we used a standard addition method where every time point

acquired had 3 standards: Standard 1: Sample + NaPP, standards 2 and 3: Sample + Mn-PP + NaPP. (See S2 in SI).

**Total Mn in suspension.** A 10 µL aliquot of an acid birnessite suspension was digested using 5.00 mL of a 100 mmol·$L^{-1}$ sodium oxalate solution and 4.99 mL of 70 % $HNO_3$, trace-metal grade.[67] The solution was thoroughly mixed, digested for 24 hours and diluted in 2% $HNO_3$ prior to analysis. Total Mn was analyzed using an Agilent 5110 Inductively Coupled Plasma – Optical Emission Spectrometry (ICP-OES) system.

**Dissolved As quantification and speciation.**

Arsenic speciation was determined using an Agilent 1260 Infinity II high-performance liquid chromatography (HPLC) system with a Hamilton PRP-X100 4.1 x 50 mm, 5 µm anion exchange column coupled to an Agilent 8900 Triple Quad Inductively Coupled Plasma - Mass Spectrometry (ICP-MS) detector. As(V) and As(III) were quantified using an isocratic flow rate of 0.3 mL·$min^{-1}$ and a mobile phase consisting of 6 mM $(NH_4)_2HPO_4$ + 6 mM $NH_4NO_3$ in 2% Methanol; As(V) and As(III) eluted at 0.56 and 3.06 minutes respectively (Figure S3.1 in SI).

As-Humic Acid (AsHA) complexes were separated using Size Exclusion Chromatography (SEC) with a Shodex OHpak SB-802.5 HQ SEC column and the same parameters described above. An isocratic flow rate at 1.0 mL·$min^{-1}$ of 50 % mobile phase 'A' (0.008 M $NaHPO_4$ + $NaH_2PO_4$), and 50 % mobile phase 'B' (0.2 M NaCl) was used.[68,69] The observed retention times were approximately 11.11 minutes for As(III) and 8.02 minutes for As-HA (Figure S3.2). Contrary to previous studies, As(V) eluted at the same retention time as As-HA.[70] To quantify the total concentration of the complexes, in addition to As(III) and As(V), the total free As ($As_T$) in solution was quantified using the same ICP-MS parameters as described above. The difference between

164 total As and the sum of As(III) plus As(V) was used to determine the complexed As; $[As]_T$ =
165 [As(V)] + [As(III)] + [AsHA].

166 **Preparation and Characterization of Humic Acid Solution.** A stock solution of HA was
167 prepared by dissolving 0.05 g of a humic acid sodium salt from Acros Organics (45-70% as HA)
168 in 10 mL of 0.1 mol·$L^{-1}$ KOH. The stock solution was diluted in 490 mL of Milli-Q water and
169 filtered through a 0.45 μm PES membrane filter, the final TOC content was measured using a GE
170 Sievers M5310C Total Organic Carbon analyzer. See section S7 in SI for details on HA
171 characterization.

172 **Kinetic Experiments.** Acid birnessite was suspended in an aqueous solution at a
173 concentration of 1.15 mmol·$L^{-1}$ (0.1 g·$L^{-1}$), in 10 mmol·$L^{-1}$ NaCl and 10 mmol·$L^{-1}$ $NaHCO_3$,
174 adjusted to pH 7.0 using a 6 mmol·$L^{-1}$ HCl solution; with a final volume of 265 mL ($HCO_3^-$ was
175 used to avoid buffer-mineral phase redox interactions[71]). Using a magnetic stirrer, the acid
176 birnessite suspension was mixed for 60 minutes to achieve uniformity. To limit microbial
177 oxidation of As(III), between 1.0 to 2.0 mL of 2% $NaN_3$ were added to the reactors.[70] The initial
178 As(III) concentration was 0.067 mmol·$L^{-1}$ (5 mg·$L^{-1}$). A 5,000 mg·$L^{-1}$ As(III) stock solution was
179 prepared from solid $NaAsO_2$, by dissolving it in 5% HCl, mixing thoroughly and filtering through
180 a 0.22 μm Nylon membrane filter. A final HA concentration of 0.83 mmolC·$L^{-1}$ (10 mgC·$L^{-1}$
181 measured as TOC) was used in all experiments. To understand the influence of HA and As(III) on
182 acid birnessite, four sets of experiments were conducted (Table 1).

183 **Table 1. Experimental sets**

| System | Description |
|---|---|

| | | |
|---|---|---|
| **No Pre-equilibration** | **As-$MnO_2$** | **Simultaneous addition of acid birnessite and As(III).** |
| | **As-$MnO_2$-HA** | **Simultaneous addition of acid birnessite, HA and As(III).** |
| **Pre-equilibration of HA with acid birnessite for 24 hours** | **(HA+$MnO_2$)+As** | **HA & $MnO_2$ pre-equilibration followed by As(III) addition**. An acid birnessite and HA suspension was prepared and left stirring for 24 hours. After which, an aliquot of As(III) stock solution was added. |
| | **HA-$MnO_2$+As** | **HA & $MnO_2$ pre-equilibration, DOM removal, followed by As(III) addition.** An acid birnessite plus HA suspension with [HA] = 3.33 mmol $C \cdot L^{-1}$ and [$MnO_2$]= 4.6 $mmol \cdot L^{-1}$ was used for the pre-equilibration period. After 24 hours, the suspension was centrifuged three times at 4000 rpm for 10 minutes, separating the supernatant after every cycle, resuspending and rinsing the solid with an aqueous solution with the same pH and ionic strength used in the batch reactor experiments until a slurry was left. It was analyzed for total Mn using ICP-OES. A given volume of this slurry was added to batch reactors, so that the total mass amount of Mn was equivalent to 1.15 $mmol \cdot L^{-1}$ of $MnO_2$. An |

| | |
|---|---|
| | aliquot of As(III) stock solution was then added into the suspension. |

Batch reactions were magnetically stirred in fluorinated ethylene propylene (FEP) containers in the dark at room temperature (22 ± 1 °C) and at least in triplicate. During the batch reactions, the containers were capped and covered with parafilm except when sampling. All experiments were conducted in the dark.

For As quantification, 200 – 250 µL were removed at the following time intervals: 1, 3, 5, 10, 20, 30, 40, 50, 60, 90, 120, 180, 240, 360, and 1440 minutes (min). The aliquots were filtered through a 0.45 µm PES membrane filter. For HPLC-ICP-MS quantification of total dissolved As, As(III), As(V) and AsHA; 50 µL of the filtered sample was diluted in 950 µL of filtered 1.0 mmol·$L^{-1}$ Na-EDTA. For Mn(III) analysis, 1.00 mL of filtered solution was collected at 2, 4, and 24 hours.

**Modeling and non-linear curve fitting.** Kinetic modeling and NLCF were done in the MATLAB R2021a software (The MathWorks Inc.) using a nonlinear least squares method with a trust-region based algorithm, a bisquare robust parameter, and the maximum number of iterations set to 400. The equation coefficients were calculated by maximizing the goodness of fit, i.e., providing the line of best fit with the highest R-square and smallest root mean square error (RMSE). The constant parameters used were [HA]=10 mg·$L^{-1}$, and $[\mathrm{As(III)}]_0/[\mathrm{As}]_0 = 1$.

NLCF was first performed on the experimentally determined concentrations of As(III) and As(V), the values for the rate constants were obtained from the fitting results and were used for the fitting of AsHA datapoints. Modeled reaction orders vary and were second order in the As,

$MnO_2$ and HA-$MnO_2$+As, while they were third order in the As-$MnO_2$-HA and (HA+$MnO_2$)+As systems. To evaluate the difference in kinetics between all systems, in accordance to the linearized plot for Langmuir-Hinshelwood kinetics, rate constants calculated are reported as pseudo-first order for all 3 As species (Section S5 in SI).[51,53] The scatter and bar plots were made using RStudio software with the ggplot2 data visualization package. The R programming language version used was 4.1.0 "Camp Pontanezen". Geochemical modeling was done in the Geochemist Workbench Community Edition software using the default LLNL thermo database.

Four different models were used, each applied to a different system. The complete derivation and conceptual figures of the reaction mechanisms can be found in SI, section S4. The simplest one was a monomolecular Langmuir-Hinshelwood (LH) mechanism, used for the reaction of a single surface-adsorbed substrate obeying a Langmuir isotherm (S4.1). The next two were based on the LH mechanism, where two adsorbed molecules react at the same sorption site, with the surface reaction being the rate-limiting step (rls). This was followed by either consecutive (LHCR) or parallel (LHPR) reaction schemes (S4.2 and S4.3). LHCR adequately described the formation of intermediates which subsequently reacted forming the final product, while LHPR described the simultaneous formation of two products. Lastly, an Eley-Rideal mechanism followed by consecutive reactions (ERCR) was used. Eley-Rideal describes the reaction between a surface-adsorbed molecule and a component in solution (S4.4).[49,53]

## RESULTS

### Batch reactions.

**Impact of dissolved HA on As(III) oxidation rate.** In the 'As-$MnO_2$' system, complete As(III) oxidation is largely complete after 90 minutes (Figure 1a); however, in the 'As-$MnO_2$-HA'

system (Figure 1b), As(III) depletion continues for more than 240 minutes. After 1440 minutes (24 hours) AsHA composes around ~14 % of the total As in solution while As(III) is completely depleted. At steady state in 'As-$MnO_2$', ~13% of total As missing (Figure 1a), this is due to adsorption of As to the mineral surface. The final pH of the suspensions increases by 0.3 in both the 'As-$MnO_2$' and 'As-$MnO_2$-HA' systems.

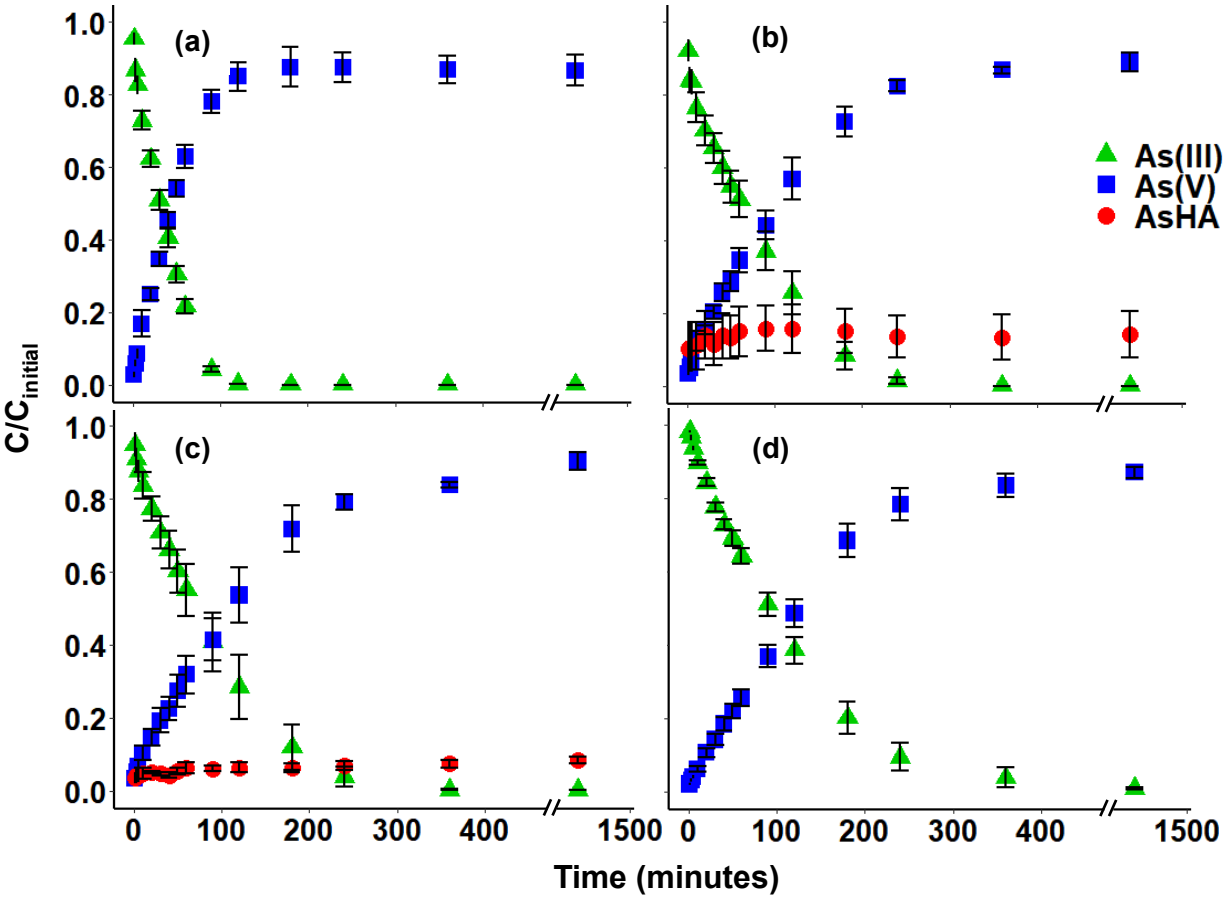


**Figure 1.** Arsenic speciation during oxidation of As(III) by acid birnessite in batch reactions in 10 mM NaCl and pH=7.00; (a) 'As-$MnO_2$'; (b) 'As-$MnO_2$-HA' (c) '(HA+$MnO_2$)+As'; (d) 'HA-$MnO_2$+As' systems. Error bars represent the standard error of the mean (SE).

**Effect of HA presorption on As(III) oxidation Rate.** For system 'As-$MnO_2$-HA', complete As(III) oxidation is complete at 240 minutes (Figure 1c); for the '(HA+$MnO_2$)+As'

system, oxidation is completed until 360 minutes (Figure 1d). During the pre-equilibration period for the '(HA+$MnO_2$)+As' and 'HA-$MnO_2$+As' systems, HA concentrations generally decrease by 2 %. After 24h, ~8 % of the total As is present as AsHA in the '(HA+$MnO_2$)+As' system (Figure 1c). Total As in solution decreases throughout the course of the 'HA-$MnO_2$+As' reaction (Figure 1d) with ~13% of total As removed at the reaction conclusion. The final pH of the '(HA+$MnO_2$)+As' system increases by 0.3 while in the 'HA-$MnO_2$+As' system, it increases by 0.5.

**Kinetic modeling.**

Non-linear curve fitting results using the Langmuir-Hinshelwood (LH) and LHCR models, of the three As species present in these systems are shown in figure 2. In Figure 2a, equations S13 and S14 are used to fit the total As-normalized concentrations As(III) and As(V) respectively. While, in Figure 2b, equations S32, S33, and S34 are used to fit normalized As(III), As(V), and AsHA respectively. The trend of the models accurately matches the concentration profiles for all systems; particularly the formation of AsHA in systems 'As-$MnO_2$-HA' and 'HA-$MnO_2$+As' (Figures 2b and 3a). The evolution of AsHA in system 'As-$MnO_2$-HA' shows a downward concavity trend, peaking at around 90 minutes further decreasing and plateauing at around 240 minutes; this is adequately described by the NLCF results of the kinetic model (Figures 2b and S6.3). Formation of AsHA in system 'HA-$MnO_2$+As'is properly described as well, showing a slight downward concavity trend in the beginning but ultimately stabilizing at around 90 minutes (Figure 3a). The r-square values ($r^2$) are included in the figure description. The fitting coefficients are shown in table 2, these correspond to a set of parameters that satisfy the general solution to the system of differential equations associated with each kinetic model (section S4 in SI).

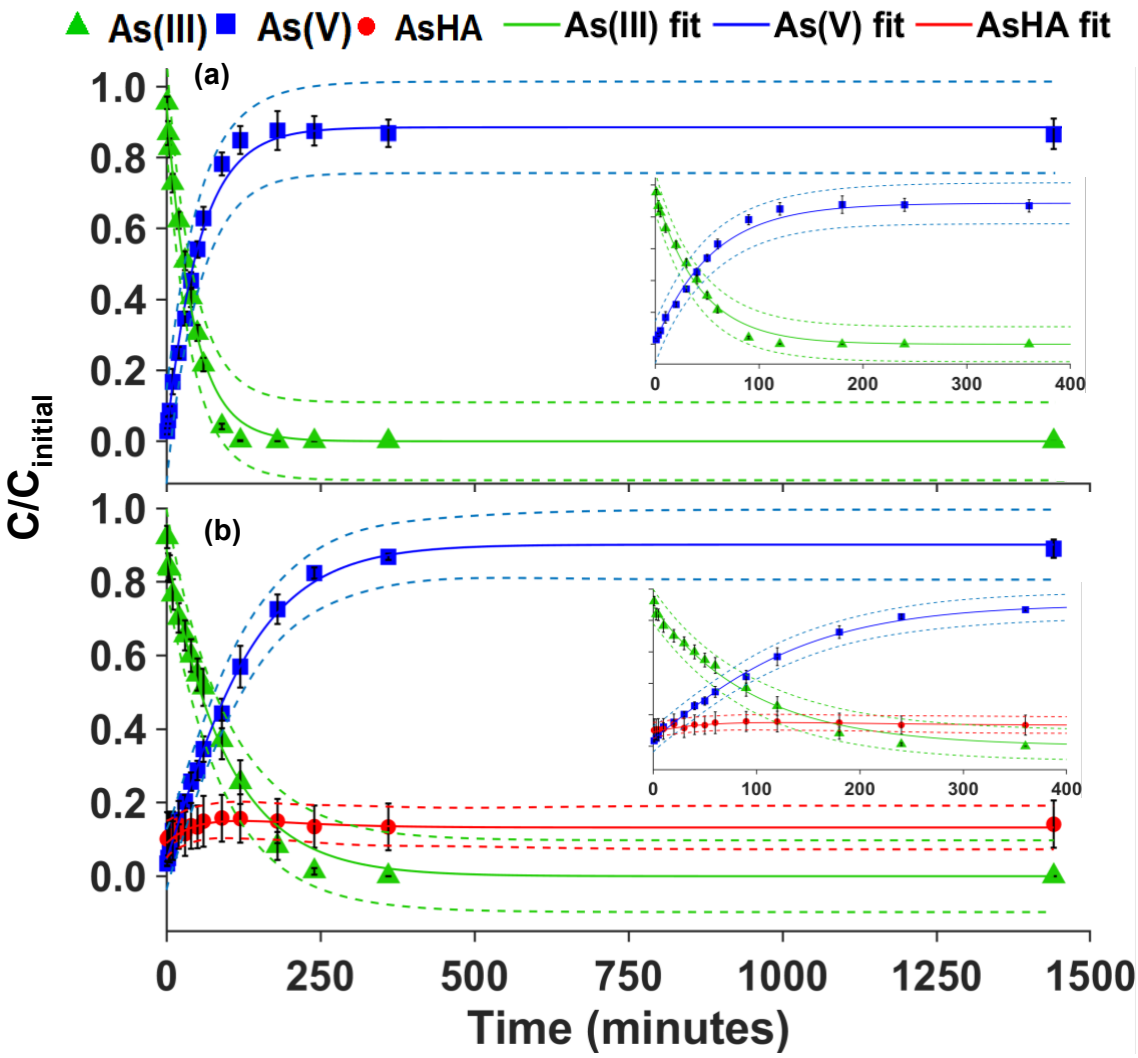


**Figure 2.** NLCF results of (a) 'As-$MnO_2$'; $r^2$=0.9916 for As(III), and 0.9923 for As(V). (b) 'As-$MnO_2$-HA'; $r^2$=0.7858 for AsHA, 0.9894 for As(III), and 0.9979 for As(V). Error bars represent SE. Dashed lines represent the color-coded 95% confidence interval (CI) of the fitted model.

The models that provide the best fit for 'As-$MnO_2$' and 'As-$MnO_2$-HA' are LH and LHCR, respectively (Figure 2). The As(III) oxidation rate constant in the 'As-$MnO_2$' system is greater than in 'As-$MnO_2$-HA' (Table 2). The models exhibit very high correlations for As(III) and As(V) concentration; however, AsHA has a much lower $r^2$ but the overall behavior of the speciation is

268 properly explained. All data points remain within the CI, giving a high degree of confidence in the
269 validity of the models. To assess the how HA present in the bulk solution impact the reaction
270 mechanism, the ERCR model is also fit to the 'As-$MnO_2$-HA' system (Figure S6.1); however, this
271 model not only exhibited a much lower $r^2$ value for the AsHA fit, but also fails to adequately
272 describe the concentration trend for this species. The better fit provided by the LHCR mechanism
273 suggests that this is the preferred pathway for the reaction.
274
275 The data for the '(HA+$MnO_2$)+As' and 'HA-$MnO_2$+As' systems are fit using LHPR
276 (equations S40 - S42.2) and LH models, respectively. These models show high correlation with
277 As(III) and As(V) (Figure 3a and 3b). Once again, AsHA has a relatively lower $r^2$ (Figures 3a and
278 S6.2a). The calculated values for the As(III) oxidation rate constants show that 'HA-$MnO_2$+As' is
279 slower than '(HA+$MnO_2$)+As' (Table 2).

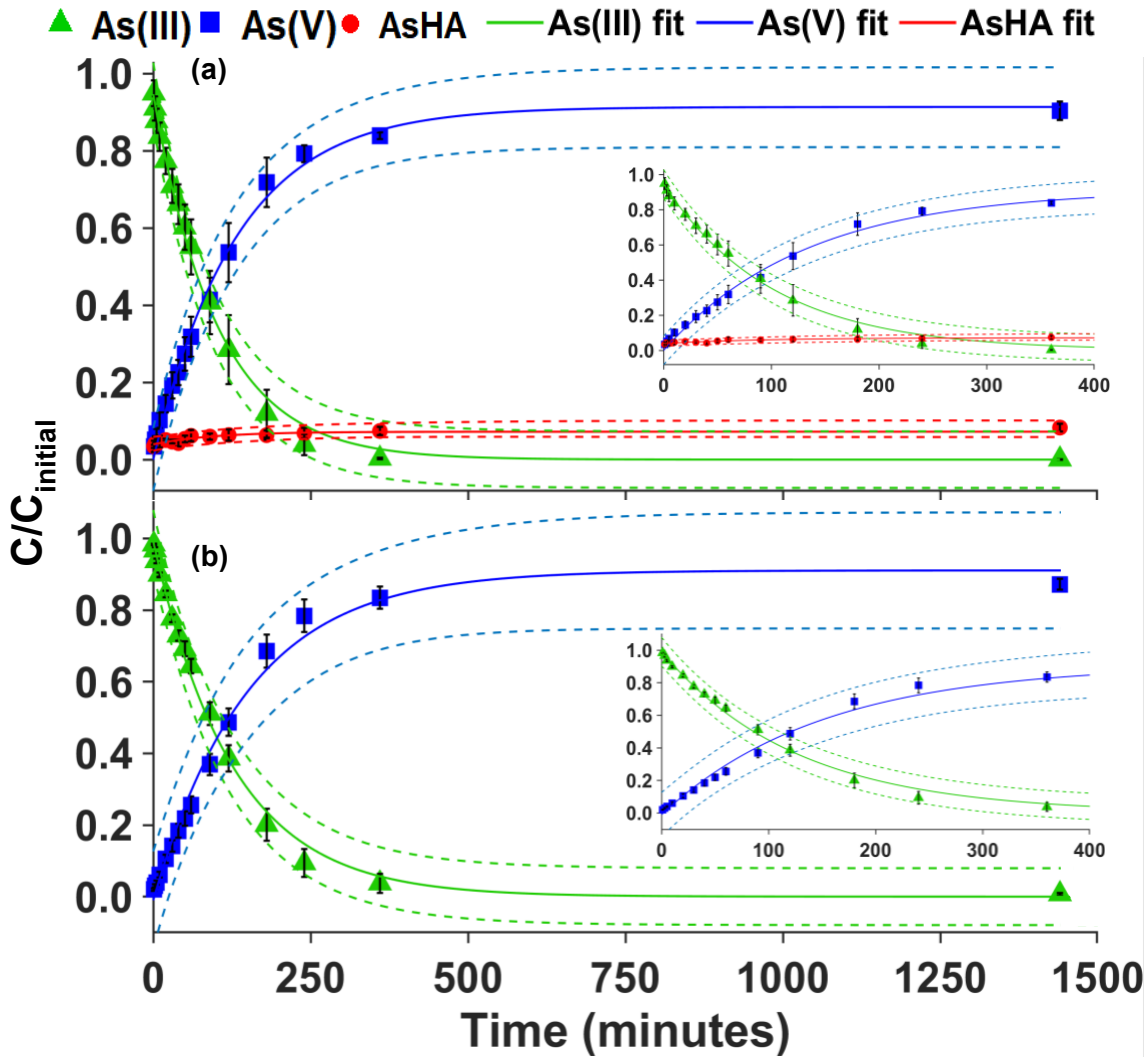


**Figure 3.** NLCF results of (a) '(HA+$MnO_2$)+As'; $r^2$=0.9946 for As(III), 0.9918 for As(V) and 0.8904 for AsHA. (b) 'HA-$MnO_2$+As'; $r^2$=0.9956 for As(III), and 0.9898 for As(V). Error bars represent SE. Dashed lines represent the color-coded 95% CI of the fitted model.

**Table 2. NLCF coefficients results with 95% confidence bounds in parenthesis**

| As-$MnO_2$-HA | | | |
|---|---|---|---|
| | **As(III)** | **As(V)** | **AsHA** |
| ***kLH*** | 0.01041 (±0.001283) | 0.01601 (±0.05978) | 0.01229 (±1.07029) |

| | | | |
|---|---|---|---|
| ***kc2*** | - | 0.01125 (±0.02273) | 0.01278 (±1.09178) |
| **C1** | 0.8893 (±0.0387) | 0.402 (±0.7603) | 0.0827 (±4.4207) |
| **C2** | - | 1.806 (±20.046) | -2.117 (±9318.117) |
| **C3** | - | - | 0.1324 (±0.0226) |
| **C4** | - | 0.9011 (±0.036) | - |

**As-$MnO_2$**

| | **As(III)** | **As(V)** |
|---|---|---|
| **C1** | 0.9535 (±0.0453) | 0.8740 (±0.0495) |
| **C2** | - | 0.8855 (±0.0366) |
| ***k*1** | 0.02349 (±0.00266) | 0.01863 (±0.00277) |

**($HA+MnO_2$)+As**

| | **As(III)** | **As(V)** | **AsHA** |
|---|---|---|---|
| ***kT*** | 0.009847 (±8.57x$10^{-4}$) | 0.007576 (±0.001128) | 0.01061 (±0.03227) |
| ***k4*** | - | 0.001718 (±2.583x$10^{4}$) | - |
| ***kLH*** | - | - | 0.5898 (±8.663x$10^{6}$) |
| **$K_2$** | - | - | 1.426 (±7.925x$10^{6}$) |
| **$K_1$** | - | - | 0.08989 (±4.667x$10^{5}$) |
| **C1** | 4.55 (±0.031) | 0 | 0.07226 (±0.01106) |

**HA-$MnO_2$+As**

| | **As(III)** | **As(V)** |
|---|---|---|
| **C1** | 0.9918 (±0.0251) | 0.9208 (±0.0658) |
| **C2** | - | 0.9107 (±0.0636) |

| | | |
|---|---|---|
| ***k1*** | 0.00796 (±0.000609) | 0.006675 (±0.001209) |

## DISCUSSION

Chemical kinetic modeling is crucial to understand the predominant reaction pathways in biogeochemical systems. Here, we use the analytical solutions of the proposed oxidation pathway to perform NLCF on experimentally determined concentration data (models are described in section S4 in SI). The final model for each system is selected based on optimization of the fitting results, i.e., highest $r^2$ and lowest RMSE. Fitting results provide values for the parameters in the final integrated equations, including the global oxidation rate constants which quantitatively demonstrates the effect HA have on the As(III) oxidation.

The conditional distribution coefficient ($K_D$) for the AsHA complexes is dependent on the concentration of As in solution.[72] At higher concentrations of As (1-5 ppm) and HA (5-30 ppm), $K_D$ becomes constant under all studied conditions, avoiding high degree of variability in results. At the selected HA and As concentrations, $K_D$ remains constant.[72] Additionally, no precipitates or the presence of different chemical species were predicted at the aforementioned experimental conditions (Figure S1.4).

For systems 'As-$MnO_2$' and 'As-$MnO_2$-HA', 'As-$MnO_2$' has the largest As(III) pseudo-first order rate constant given that there is no presence of HA to inhibit oxidation (Table 2). The decrease of the oxidation rate constant with the addition of HA is an indication that the HA molecules are limiting the reaction by blocking the active surface sites of the mineral phase.[35,73] The best fit from monomolecular LH in the 'As-$MnO_2$' (Figure 1a) data indicates that As(III) oxidation proceeds via sorption, electron-transfer at the $MnO_2$ surface, and desorption of As(V) (S4.1). For 'As-$MnO_2$-HA', the LHCR model fits the data best (Figure 2b); thus, suggesting that

As(III) oxidation proceeds via a reaction mechanism where adsorbed As(III) is oxidized and then complexed by HA on $MnO_2$ surface, followed by desorption and dissociation of AsHA to form As(V) (S4.2 in SI). Datapoints are within the 95% CI, giving a high degree of confidence in the validity of the model. The second order rate constant for As(III) oxidation in 'As-$MnO_2$' equals 14.1 $L \cdot g^{-1} \cdot h^{-1}$ (or 0.55 $L \cdot m^{-2} \cdot h^{-1}$ in terms of surface area), well within reported values under similar conditions.[1,45] Feng et al. (2018) reported that As(III) oxidation and As(V) desorption proceed with similar reaction rates in a system similar to 'As-$MnO_2$';[54] to evaluate the individual contribution of oxidation and desorption in the concerted reaction ($k_2$), we can obtain their approximate values from the rate constant ($k_{oxidation} \approx k_{desorption} \approx 0.5k_2$).

The ERCR model is also applied in 'As-$MnO_2$-HA', but the results suggest that HA present in solution has only a minor contribution in the overall mechanism, particularly over longer time periods. The fitted curve for AsHA initially shows good correlation with the data from 0 to 360 minutes but the model fails to accurately describe the data point at 24 hours, since the model predicts an exponential decay in AsHA (Figure S6.1). The better fit provided by the LH and LHCR models leads us to conclude that the reactions most likely occur via these two pathways.

The calculated As(III) oxidation rate constants for '(HA+$MnO_2$)+As' and 'As-$MnO_2$-HA' are similar; this could be due to similarities in the reaction mechanisms (Figure 4). The As(III) oxidation rate constant in the 'HA-$MnO_2$+As' system is almost 3 times lower than the comparable 'As-$MnO_2$' system (Table 2), where no HA is present in solution. The possibility of competing reactions exists; even though LHPR (S4.3) provides the best fit for the '(HA+$MnO_2$)+As' system, the concentration profile for AsHA (Figure 1c) clearly shows a concave down trend in the first 40 minutes, showing the reaction initially follows an LHCR trend (Figures S6.2a and S6.2b). The similar values for the rate constants could also be an indication that the effect of HA on the active

surface sites of the acid birnessite is independent of the exposure time; rather the complexation of As proves to have a more important effect.

During the 24-hour pre-adsorption period, the concentration of HA decreased by 2 %, while $MnO_2$ surface reactivity is modified (Figure 1); this indicates that a portion of HA remain adsorbed on the surface of minerals. There is a passivation effect that drastically decreases the rate at which As(III) is oxidized on the surface of acid birnessite without forming aqueous AsHA.[26,32,73] The impact HA has on the surface of the birnessite is mainly via the occupation of active surface sites where oxidation occurs; in addition to the formation of AsHA, but only in environments where HA concentration is high enough.[73] This surface fouling is characteristic of NOM-coated minerals; which affects the behavior of pure mineral surfaces.[13,73]

In systems with pre-adsorbed HA to solids, formation of AsHA enhances As partitioning into solution from solid phases.[68,19,13] However, in the system where HA is pre-equilibrated with the mineral surface ('HA-$MnO_2$+As'), a decrease in total As in solution is observed, suggesting As sorption in the form of AsHA complexes on the HA-coated $MnO_2$ surface.[32] No AsHA nor HA (i.e., TOC= 0 $mg \cdot L^{-1}$) is detected in solution, indicating that desorption of either species does not take place. Saada et al.(2003) reports that adsorbed humic substances onto a Ca-exchanged kaolinite significantly impact As(V) sorption, increasing its partitioning into the solids.[26] Thus, the HA-amended $MnO_2$ surface seems to limit the partitioning of As to aqueous phase by forming surface-bound As-HA complexes. Since adsorption is the initial step of all presented mechanisms, this effect is also observed when comparing pseudo-first order oxidation rate constants. In systems where HA are present, there is a sharp decrease in the value of the rate constants compared to the 'As-$MnO_2$' system (Figure 4).

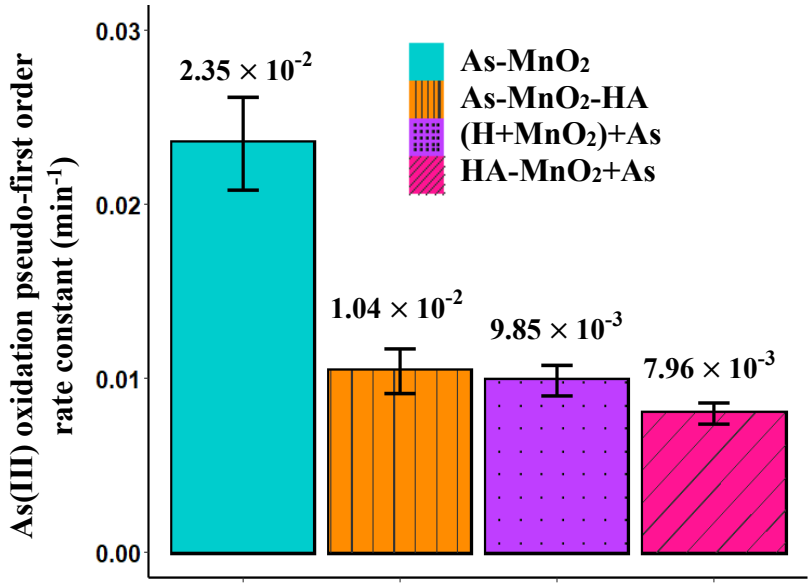


**Figure 4.** Pseudo-first order oxidation rate constants of As(III) in the four different systems. Error bars represent 95% confidence intervals.

**Reaction mechanisms.**

**'As-$MnO_2$' and 'HA-$MnO_2$+As'.** The formation of AsHA was not observed in these systems, hence they were fit with the monomolecular Langmuir-Hinshelwood model (Figures 5 and S4.1). The expression for the overall reaction is modelled after classic kinetics of reactions on surfaces (Equation 1).[49]

$$\mathrm{As(III)(aq) + MnO_2(s) \overset{k_1}{\underset{k_{-1}}{\rightleftharpoons}} As \equiv MnO_2(s) \xrightarrow{k_2} As(V)(aq) + Mn^{III/IV}O_2(s)} \quad (1)$$

**'As-$MnO_2$-HA'.** The best fitting results were obtained using the LHCR model, where the oxidation reaction proceeds through 2 main sets of reactions (SI section S4.2). Briefly, the first is via a simplified bimolecular LH mechanism between As(V) and HA adsorbed on $MnO_2$. Starting with a concerted reaction of As(III) oxidation, complexation of adsorbed As(V) by HA, and

desorption (Figure 5). The global LH reaction has a second order rate constant equal to $k_{LH}$ (Equation S28 in SI). The second reaction involves the dissociation of AsHA into aqueous As(V) and with a rate constant equal to $k_{c2}$ (Equation 2).

$$\mathrm{As(III)(aq) + HA\ (aq) + 2MnO_2(s) \xrightarrow{k_{LH}} AsHA(aq) + 2Mn^{III/IV}O_2(s) \xrightarrow{k_{c2}} As(V)(aq) + 2Mn^{III/IV}O_2(s) + HA\ (aq)} \quad (2)$$

**'(HA+$MnO_2$)+As'.** When HA is pre-adsorbed to the mineral surface (HA≡$MnO_2$) and remaining the main mechanism involves two competitive pseudo-first order steps (Equations 3 and 4). It was fit using LHPR model (SI section S4.3) consisting of two competitive steps, where adsorbed As(III) is oxidized on the $MnO_2$ surface; it is then followed by As(V) desorption or formation and desorption of AsHA (Figure 5).

$$\mathrm{As(III)(aq) + HA(aq) + 2MnO_2(s) \xrightarrow{k_{LH}} AsHA(aq) + 2Mn^{III/IV}O_2(s)} \quad (3)$$

$$\mathrm{As(III)(aq) + 2MnO_2(s) \xrightarrow{k_4} As(V)(aq) + 2Mn^{III/IV}O_2(s)} \quad (4)$$

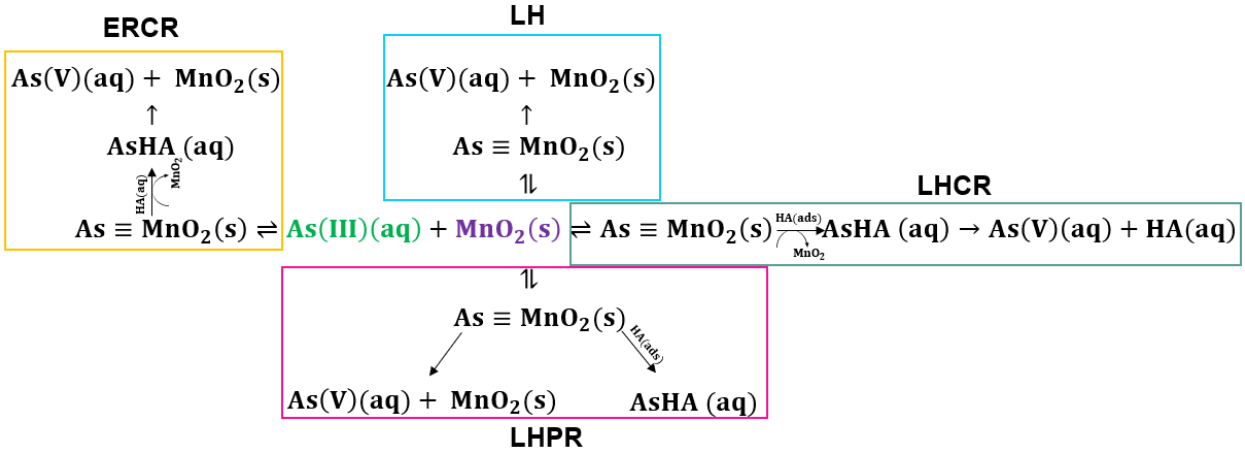

**Figure 5.** General reaction schemes for LH, LHCR, LHPR, and ERCR mechanisms.

**Mn(III) formation.**

In all studied systems, Mn acts as a competitive adsorbate, blocking active sites. In a stirred-flow system where As(III) oxidation by at δ-$MnO_2$ (a phyllomanganate similar to acid birnessite) is studied in the absence of HA, Mn(II) sorbs at vacant sites and a portion reacts with Mn(IV) to form Mn(III).[35] During As(III) oxidation, $Mn^{2+}$ adsorbs at the acid birnessite vacant sites where it can react with Mn(IV) forming Mn(III).[35,74,75,76] Dissolved Mn(III) concentration increases within the first 4 hours of reaction, followed by a slight decrease between 0.01-0.03 $mmol \cdot L^{-1}$ (Figures 6a and 6b) or increase of 0.13 $mmol \cdot L^{-1}$ (Figure 6c). It is clear that dissolved Mn(III) concentration is higher in the systems with HA in solution (Figures 6a and 6c). This could be caused by the HA complexing $Mn^{3+}$, thus forming stable Mn(III)-HA complexes and hindering its adsorption or dismutation.[73,77] Given that oxidation of organic matter by Mn oxides is a major pathway, formation of Mn(III) could be ascribed to reduction of $MnO_2$ by HA.[37,78] Nevertheless, at high concentrations (10 $mg \cdot L^{-1}$), HA exhibit an inhibiting effect on $MnO_2$, acting as competitors occupying active sites on the surface of $MnO_2$.[73]

The observed concentration trend is similar to the one simulated by Nesbitt et al. (1998), confirming the origin of Mn(III) to be in the near-surface of birnessite.[40] The HA-$MnO_2$+As system exhibits the lowest concentrations, remaining constant with little variability; this shows that lack of HA in solution has a negative impact on the stability of $Mn^{3+}$, reaching a maximum concentration of 0.24 $mmol \cdot L^{-1}$ (Figure 6d). Furthermore, amendment of the $MnO_2$ surface during the pre-equilibration period reduces the amount of Mn(III) generated (Figures 6a and 6d).

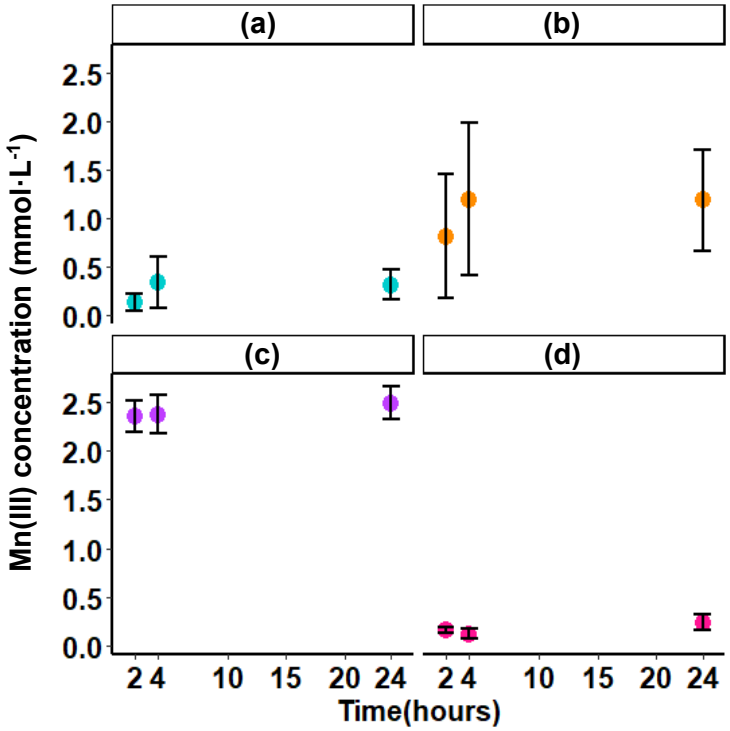


401

402 **Figure 6.** Concentration of Mn(III) in solution (a) 'As-$MnO_2$'; (b) 'As-$MnO_2$-HA' (c)
403 '(HA+$MnO_2$)+As'; (d) 'HA-$MnO_2$+As'. Error bars represent propagated uncertainty for each
404 measurement.

405

406 Even though (HA+$MnO_2$)+As has a higher Mn(III) concentration (Figure 6c), it does not
407 correlate with a higher AsHA concentration (Figure 1c) compared to As-$MnO_2$-HA (Figure 1b).
408 This suggests that Mn(III) does not have a significant effect in As complexation in the form of a
409 bridging complex.

410

411 **ENVIRONMENTAL IMPLICATIONS.** This study provides a detailed description of
412 environmentally relevant, surface-catalyzed electron transfer reactions in the presence of organic
413 matter. The impact HA have on As(III) oxidation catalyzed by acid birnessite is not only limited
414 to passivation of the surface; but also, complexation. The results of this study demonstrate the

415 influence of HA on As speciation. The main environmental implication is that exposure of HA to
416 mineral surfaces sharply decreases As(III) oxidation rate, likely due to occupation of active sites
417 at the surface of $MnO_2$. The observed pseudo-first order rate constants differ from other studies on
418 account of the complexity of the mechanism, yet fall within the expected range of values for the
419 initial conditions.[1,45] It must be considered that multiple reactions can occur simultaneously, both
420 LH and ER mechanisms are plausible in these systems.

421 Here we thoroughly derive a set of mathematical models, based on LH kinetics, and
422 provide analytical solutions that enable an in-depth description of complex binary and ternary
423 systems, i.e., As(III) oxidation with $MnO_2$ in the presence and absence of HA. With the rigorously
424 described reaction mechanisms, we can accurately describe the reaction at any point in time and
425 assess As speciation (adsorption, oxidation, and complexation). Additionally, it is no longer
426 necessary to approximate the oxidation of As(III) with a Mn oxide using pseudo-first order
427 conditions, nor to limit to the evaluation of initial reaction rates followed by calculation of second
428 order rate constants; these approaches are limited to short time periods at the beginning of the
429 reaction, severely restricting its applicability.[45]

430 This study provides a better understanding regarding As-HA interactions; and thus validate
431 the consideration of AsHA complexes in geochemical models for contaminant transport and
432 remediation strategies. Moreover, the models presented here are significant quantitative tools for
433 predicting As speciation kinetics in natural aqueous environments. Furthermore, we demonstrate
434 the functionality of the proposed reaction mechanisms; their applicability to the As/$MnO_2$/HA
435 systems will prove useful for future studies. For instance, their possible application to describe
436 solid-mediated electron transfer reactions of other contaminants in aqueous solutions in the
437 presence of mineral surfaces. There has been an increasing trend of using Mn oxides for water

treatment, particularly in adsorption studies.[79] The potential use of Mn oxides in bulk scale for remediation of complex matrices, e.g., wastewater, requires a detailed mechanistic knowledge, which we believe this study provides.

**Supporting Information:** Chemicals and materials; XRD spectra, SEM images, and PZC determination of acid birnessite; log[$As(OH)_4^-$] – pH speciation diagram; Mn(III) quantification; HPLC-ICP-MS, and SEC-ICP-MS chromatograms; LOD and LOQ for HPLC-ICP-MS quantification of As; monomolecular LH mechanism; LHCR mechanism; LHPR mechanism; ERCR mechanism; pseudo-first order rate constants for all mechanisms; additional modeling results; and characterization of HA.

## ACKNOWLEDGMENTS

The authors appreciate the constructive comments and suggestions of four anonymous reviewers. The authors thank James Lazarcik for the laboratory assistance, Anna Beth Thomas for help in acid birnessite synthesis, and Dr. Jorge Arturo Campos González-Angulo for helpful advice and guidance when performing curve fitting. David is grateful for funding provided by the Graduate Engineering Research Scholars (GERS) from the University of Wisconsin-Madison. This research was funded by the National Science Foundation CAREER Program Grant (EAR 1846851).

## REFERENCES

(1) Schacht, L.; Ginder-Vogel, M. Arsenite Depletion by Manganese Oxides: A Case Study on the Limitations of Observed First Order Rate Constants. *Soil Syst.* **2018**, *2* (3), 39. https://doi.org/10.3390/soilsystems2030039.

(2) *USGS. Arsenic and Drinking Water*. https://www.usgs.gov/mission-areas/water-resources/science/arsenic-and-drinking-water?qt-science_center_objects=0#qt-science_center_objects (accessed 2023-02-09).

(3) Shaji, E.; Santosh, M.; Sarath, K. V.; Prakash, P.; Deepchand, V.; Divya, B. V. Arsenic Contamination of Groundwater: A Global Synopsis with Focus on the Indian Peninsula.

*Geosci. Front.* **2021**, *12* (3), 101079. https://doi.org/10.1016/j.gsf.2020.08.015.

(4) Podgorski, J.; Berg, M. Global Threat of Arsenic in Groundwater. *Science* **2020**, *368* (6493), 845–850. https://doi.org/10.1126/science.aba1510.

(5) Amen, R.; Bashir, H.; Bibi, I.; Shaheen, S. M.; Niazi, N. K.; Shahid, M.; Hussain, M. M.; Antoniadis, V.; Shakoor, M. B.; Al-Solaimani, S. G.; Wang, H.; Bundschuh, J.; Rinklebe, J. A Critical Review on Arsenic Removal from Water Using Biochar-Based Sorbents: The Significance of Modification and Redox Reactions. *Chem. Eng. J.* **2020**, *396* (November 2019). https://doi.org/10.1016/j.cej.2020.125195.

(6) International Agency for Research on Cancer. Arsenic and Arsenic Compounds. *IARC Monogr.* **2012**, *100C*, 41–93.

(7) World Health Organization. Exposure to Arsenic: A Major Public Health Concern. 2010, p 5.

(8) Qian, G.; Xu, L.; Li, N.; Wang, K.; Qu, Y.; Xu, Y. Enhanced Arsenic Migration in Tailings Soil with the Addition of Humic Acid, Fulvic Acid and Thiol-Modified Humic Acid. *Chemosphere* **2022**, *286* (August 2021). https://doi.org/10.1016/j.chemosphere.2021.131784.

(9) Kim, E. J.; Yoo, J. C.; Baek, K. Arsenic Speciation and Bioaccessibility in Arsenic-Contaminated Soils: Sequential Extraction and Mineralogical Investigation. *Environ. Pollut.* **2014**, *186*, 29–35. https://doi.org/10.1016/j.envpol.2013.11.032.

(10) Zhao, F.-J.; Mcgrath, S. P.; Meharg, A. A. Arsenic as a Food Chain Contaminant: Mechanisms of Plant Uptake and Metabolism and Mitigation Strategies. *Annu. Rev. Plant Biol.* **2010**, *61* (1), 535–559. https://doi.org/10.1146/annurev-arplant-042809-112152.

(11) Smedley, P. L.; Kinniburgh, D. G. A Review of the Source, Behaviour and Distribution of Arsenic in Natural Waters. *Appl. Geochemistry* **2002**, *17* (5), 517–568. https://doi.org/10.1016/S0883-2927(02)00018-5.

(12) Redman, A. D.; Macalady, D. L.; Ahmann, D. Natural Organic Matter Affects Arsenic Speciation and Sorption onto Hematite. *Environ. Sci. Technol.* **2002**, *36* (13), 2889–2896. https://doi.org/10.1021/es0112801.

(13) Wang, S.; Mulligan, C. N. Effect of Natural Organic Matter on Arsenic Release from Soils and Sediments into Groundwater. *Environ. Geochem. Health* **2006**, *28* (3), 197–214. https://doi.org/10.1007/s10653-005-9032-y.

(14) Villalobos, M.; Escobar-Quiroz, I. N.; Salazar-Camacho, C. The Influence of Particle Size and Structure on the Sorption and Oxidation Behavior of Birnessite: I. Adsorption of As(V) and Oxidation of As(III). *Geochim. Cosmochim. Acta* **2014**, *125*, 564–581. https://doi.org/10.1016/j.gca.2013.10.029.

(15) Mohan, D.; Pittman, C. U. Arsenic Removal from Water/Wastewater Using Adsorbents-A Critical Review. *J. Hazard. Mater.* **2007**, *142* (1–2), 1–53. https://doi.org/10.1016/j.jhazmat.2007.01.006.

(16) Wu, Y.; Li, W.; Sparks, D. L. Effect of Iron(II) on Arsenic Sequestration by δ-MnO2:

Desorption Studies Using Stirred-Flow Experiments and X-Ray Absorption Fine-Structure Spectroscopy. *Environ. Sci. Technol.* **2015**, *49* (22), 13360–13368. https://doi.org/10.1021/acs.est.5b04087.

(17) Wu, Y.; Li, W.; Sparks, D. L. The Effects of Iron(II) on the Kinetics of Arsenic Oxidation and Sorption on Manganese Oxides. *J. Colloid Interface Sci.* **2015**, *457*, 319–328. https://doi.org/10.1016/j.jcis.2015.07.022.

(18) Sparks, D. L. *Environmental Soil Chemistry*, Second edi.; Elsevier, 2003. https://doi.org/10.1016/B978-0-12-656446-4.X5000-2.

(19) Wang, S.; Mulligan, C. N. Enhanced Mobilization of Arsenic and Heavy Metals from Mine Tailings by Humic Acid. *Chemosphere* **2009**, *74* (2), 274–279. https://doi.org/10.1016/j.chemosphere.2008.09.040.

(20) Sharma, P.; Rolle, M.; Kocar, B.; Fendorf, S.; Kappler, A. Influence of Natural Organic Matter on as Transport and Retention. *Environ. Sci. Technol.* **2011**, *45* (2), 546–553. https://doi.org/10.1021/es1026008.

(21) Biswas, A.; Besold, J.; Sjöstedt, C.; Gustafsson, J. P.; Scheinost, A. C.; Planer-Friedrich, B. Complexation of Arsenite, Arsenate, and Monothioarsenate with Oxygen-Containing Functional Groups of Natural Organic Matter: An XAS Study. *Environ. Sci. Technol.* **2019**, *53* (18), 10723–10731. https://doi.org/10.1021/acs.est.9b03020.

(22) Sposito, G. *The Chemistry of Soils*, Second.; Oxford University Press: New York, 2008.

(23) Kong, S.; Wang, Y.; Zhan, H.; Liu, M.; Liang, L.; Hu, Q. Competitive Adsorption of Humic Acid and Arsenate on Nanoscale Iron-Manganese Binary Oxide-Loaded Zeolite in Groundwater. *J. Geochemical Explor.* **2014**, *144*, 220–225. https://doi.org/10.1016/j.gexplo.2014.02.005.

(24) Fuller, C. C.; Davis, J.; Waychunas, G. Surface Chemistry of Ferrihydrite: Part 2. Kinetics of Arsenate Adsorption and Coprecipitation. *Geochem. Trans.* **1993**, *57*, 2271–2281. https://doi.org/10.3998/mpub.168625.

(25) Buschmann, J.; Kappeler, A.; Lindauer, U.; Kistler, D.; Berg, M.; Sigg, L. Arsenite and Arsenate Binding to Dissolved Humic Acids: Influence of PH, Type of Humic Acid, and Aluminum. *Environ. Sci. Technol.* **2006**, *40* (19), 6015–6020. https://doi.org/10.1021/es061057+.

(26) Saada, A.; Breeze, D.; Crouzet, C.; Cornu, S.; Baranger, P. Adsorption of Arsenic (V) on Kaolinite and on Kaolinite-Humic Acid Complexes Role of Humic Acid Nitrogen Groups. *Chemosphere* **2003**, *51* (8), 757–763. https://doi.org/10.1016/S0045-6535(03)00219-4.

(27) Wang, S.; Mulligan, C. N. Effect of Natural Organic Matter on Arsenic Mobilization from Mine Tailings. *J. Hazard. Mater.* **2009**, *168* (2–3), 721–726. https://doi.org/10.1016/j.jhazmat.2009.02.088.

(28) Zecchin, S.; Crognale, S.; Zaccheo, P.; Fazi, S.; Amalfitano, S.; Casentini, B.; Callegari, M.; Zanchi, R.; Sacchi, G. A.; Rossetti, S.; Cavalca, L. Adaptation of Microbial Communities to Environmental Arsenic and Selection of Arsenite-Oxidizing Bacteria From Contaminated Groundwaters. *Front. Microbiol.* **2021**, *12*.

https://doi.org/10.3389/fmicb.2021.634025.

(29) Henke, K. R. *Arsenic: Environmental Chemistry, Health Threats and Waste Treatment*; Wiley, 2009. https://doi.org/10.1002/9780470741122.

(30) Costa, A. S. P. N.; Nascimento, A. L. A.; Botero, W. G.; Carvalho, C. M.; Tonholo, J.; Santos, J. C. C.; Anunciação, D. S. Interaction between Humic Substances and Arsenic Species Simulating Environmental Conditions. *Sci. Total Environ.* **2022**, *802*, 149779. https://doi.org/10.1016/j.scitotenv.2021.149779.

(31) Yi, X. Y.; Yang, Y. P.; Yuan, H. Y.; Chen, Z.; Duan, G. L.; Zhu, Y. G. Coupling Metabolisms of Arsenic and Iron with Humic Substances through Microorganisms in Paddy Soil. *J. Hazard. Mater.* **2019**, *373* (December 2018), 591–599. https://doi.org/10.1016/j.jhazmat.2019.03.113.

(32) Thanabalasingam, P.; Pickering, W. F. Arsenic Sorption by Humic Acids. *Environ. Pollution. Ser. B, Chem. Phys.* **1986**, *12* (3), 233–246. https://doi.org/10.1016/0143-148X(86)90012-1.

(33) Remucal, C. K.; Ginder-Vogel, M. A Critical Review of the Reactivity of Manganese Oxides with Organic Contaminants. *Environ. Sci. Process. Impacts* **2014**, *16* (6), 1247–1266. https://doi.org/10.1039/c3em00703k.

(34) Lafferty, B. J.; Ginder-Vogel, M.; Sparks, D. L. Arsenite Oxidation by a Poorly Crystalline Manganese-Oxide 1. Stirred-Flow Experiments. *Environ. Sci. Technol.* **2010**, *44* (22), 8460–8466. https://doi.org/10.1021/es102013p.

(35) Lafferty, B. J.; Ginder-Vogel, M.; Zhu, M.; Livi, K. J. T. T.; Sparks, D. L. Arsenite Oxidation by a Poorly Crystalline Manganese-Oxide. 2. Results from X-Ray Absorption Spectroscopy and X-Ray Diffraction. *Environ. Sci. Technol.* **2010**, *44* (22), 8467–8472. https://doi.org/10.1021/es102016c.

(36) Gu, B.; Schmitt, J.; Chen, Z.; Liang, L.; McCarthy, J. F. Adsorption and Desorption of Natural Organic Matter on Iron Oxide: Mechanisms and Models. *Environ. Sci. Technol.* **1994**, *28* (1), 38–46. https://doi.org/10.1021/es00050a007.

(37) Trainer, E. L.; Ginder-Vogel, M.; Remucal, C. K. Selective Reactivity and Oxidation of Dissolved Organic Matter by Manganese Oxides. *Environ. Sci. Technol.* **2021**, *55* (17), 12084–12094. https://doi.org/10.1021/acs.est.1c03972.

(38) Zhang, J.; Mckenna, A. M.; Zhu, M. Macromolecular Characterization of Compound Selectivity for Oxidation and Oxidative Alterations of Dissolved Organic Matter by Manganese Oxide. *Environ. Sci. Technol.* **2021**, *55* (11), 7741–7751. https://doi.org/10.1021/acs.est.1c01283.

(39) Scott, M. J.; Morgan, J. J. Reactions at Oxide Surfaces. 1. Oxidation of As(III) by Synthetic Birnessite. *Environ. Sci. Technol.* **1995**, *29* (8), 1898–1905. https://doi.org/10.1021/es00008a006.

(40) Nesbitt, H. W.; Canning, G. W.; Bancroft, G. M. XPS Study of Reductive Dissolution of 7Å-Birnessite by H3AsO3, with Constraints on Reaction Mechanism. *Geochim. Cosmochim. Acta* **1998**, *62* (12), 2097–2110. https://doi.org/10.1016/S0016-

7037(98)00146-X.

(41) Rathi, B.; Jamieson, J.; Sun, J.; Siade, A. J.; Zhu, M.; Cirpka, O. A.; Prommer, H. Process-Based Modeling of Arsenic(III) Oxidation by Manganese Oxides under Circumneutral PH Conditions. *Water Res.* **2020**, *185*, 116195. https://doi.org/10.1016/j.watres.2020.116195.

(42) Ying, S. C.; Kocar, B. D.; Griffis, S. D.; Fendorf, S. Competitive Microbially and Mn Oxide Mediated Redox Processes Controlling Arsenic Speciation and Partitioning. *Environ. Sci. Technol.* **2011**, *45* (13), 5572–5579. https://doi.org/10.1021/es200351m.

(43) Driehaus, W.; Seith, R.; Jekel, M. Oxidation of Arsenate(III) with Manganese Oxides in Water Treatment. *Water Res.* **1995**, *29* (1), 297–305. https://doi.org/10.1016/0043-1354(94)E0089-O.

(44) Mitsunobu, S.; Takahashi, Y.; Uruga, T. Observation of Chemical Reactions at the Solid-Water Interface by Quick XAFS Combined with a Column Reactor. *Anal. Chem.* **2006**, *78* (19), 7040–7043. https://doi.org/10.1021/ac060961h.

(45) Owings, S. M.; Luther, G. W.; Taillefert, M. Development of a Rate Law for Arsenite Oxidation by Manganese Oxides. *Geochim. Cosmochim. Acta* **2019**, *250*, 251–267. https://doi.org/10.1016/j.gca.2019.02.003.

(46) Manning, B. A.; Fendorf, S. E.; Bostick, B.; Suarez, D. L. Arsenic(III) Oxidation and Arsenic(V) Adsorption Reactions on Synthetic Birnessite. *Environ. Sci. Technol.* **2002**, *36* (5), 976–981. https://doi.org/10.1021/es0110170.

(47) Fischel, M. H. H.; Fischel, J. S.; Lafferty, B. J.; Sparks, D. L. The Influence of Environmental Conditions on Kinetics of Arsenite Oxidation by Manganese-Oxides. *Geochem. Trans.* **2015**, *16* (1), 1–10. https://doi.org/10.1186/s12932-015-0030-4.

(48) Haynes, A. Concepts of Modern Catalysis and Kinetics. *Synthesis (Stuttg).* **2005**, *2005* (05), 851–851. https://doi.org/10.1055/s-2005-866709.

(49) Arnaut, L.; Formosinho, S.; Burrows, H. *Chemical Kinetics From Molecular Structure to Chemical Reactivity*, 1st ed.; Elsevier Science, 2007.

(50) Endalew, A. K.; Kiros, Y.; Zanzi, R. Inorganic Heterogeneous Catalysts for Biodiesel Production from Vegetable Oils. *Biomass and Bioenergy* **2011**, *35* (9), 3787–3809. https://doi.org/10.1016/j.biombioe.2011.06.011.

(51) Kumar, K. V.; Porkodi, K.; Rocha, F. Langmuir-Hinshelwood Kinetics - A Theoretical Study. *Catal. Commun.* **2008**, *9* (1), 82–84. https://doi.org/10.1016/j.catcom.2007.05.019.

(52) Mark E. Davis; Davis, R. J. Chapter 5: Heterogeneous Catalysis. In *Fundamentals of Chemical Reaction Engineering*; Dover Publications Inc., 2003; Vol. 54, pp 133–171. https://doi.org/10.1002/anie.201410738.

(53) Ohtani, B. *Photocatalysis by Inorganic Solid Materials: Revisiting Its Definition, Concepts, and Experimental Procedures*, 1st ed.; Elsevier Inc., 2011; Vol. 63. https://doi.org/10.1016/B978-0-12-385904-4.00001-9.

(54) Feng, X.; Wang, P.; Shi, Z.; Kwon, K. D.; Zhao, H.; Yin, H.; Lin, Z.; Zhu, M.; Liang, X.; Liu, F.; Sparks, D. L. A Quantitative Model for the Coupled Kinetics of Arsenic

622 Adsorption/Desorption and Oxidation on Manganese Oxides. *Environ. Sci. Technol. Lett.*
623 **2018**, *5* (3), 175–180. https://doi.org/10.1021/acs.estlett.8b00058.

624 (55) Hua, J. Adsorption of Low-Concentration Arsenic from Water by Co-Modified Bentonite
625 with Manganese Oxides and Poly(Dimethyldiallylammonium Chloride). *J. Environ. Chem.*
626 *Eng.* **2018**, *6* (1), 156–168. https://doi.org/10.1016/j.jece.2017.11.062.

627 (56) McKenzie, R. M. The Synthesis of Birnessite, Cryptomelane, and Some Other Oxides and
628 Hydroxides of Manganese. *Mineral. Mag.* **1971**, *38* (296), 493–502.
629 https://doi.org/10.1180/minmag.1971.038.296.12.

630 (57) Balgooyen, S.; Alaimo, P. J.; Remucal, C. K.; Ginder-Vogel, M. Structural Transformation
631 of MnO2 during the Oxidation of Bisphenol A. *Environ. Sci. Technol.* **2017**, *51* (11), 6053–
632 6062. https://doi.org/10.1021/acs.est.6b05904.

633 (58) Villalobos, M.; Toner, B.; Bargar, J.; Sposito, G. Characterization of the Manganese Oxide
634 Produced by Pseudomonas Putida Strain MnB1. *Geochim. Cosmochim. Acta* **2003**, *67* (14),
635 2649–2662. https://doi.org/10.1016/S0016-7037(03)00217-5.

636 (59) Yin, H.; Liu, F.; Feng, X.; Hu, T.; Zheng, L.; Qiu, G.; Koopal, L. K.; Tan, W. Effects of Fe
637 Doping on the Structures and Properties of Hexagonal Birnessites - Comparison with Co
638 and Ni Doping. *Geochim. Cosmochim. Acta* **2013**, *117*, 1–15.
639 https://doi.org/10.1016/j.gca.2013.04.020.

640 (60) Gao, T.; Shen, Y.; Jia, Z.; Qiu, G.; Liu, F.; Zhang, Y.; Feng, X.; Cai, C. Interaction
641 Mechanisms and Kinetics of Ferrous Ion and Hexagonal Birnessite in Aqueous Systems.
642 *Geochem. Trans.* **2015**, *16* (1), 1–14. https://doi.org/10.1186/s12932-015-0031-3.

643 (61) Liu, Q.; Zhong, L. Bin; Zhao, Q. B.; Frear, C.; Zheng, Y. M. Synthesis of
644 Fe3O4/Polyacrylonitrile Composite Electrospun Nanofiber Mat for Effective Adsorption of
645 Tetracycline. *ACS Appl. Mater. Interfaces* **2015**, *7* (27), 14573–14583.
646 https://doi.org/10.1021/acsami.5b04598.

647 (62) Yazdani, M. R.; Virolainen, E.; Conley, K.; Vahala, R. Chitosan-Zinc(II) Complexes as a
648 Bio-Sorbent for the Adsorptive Abatement of Phosphate: Mechanism of Complexation and
649 Assessment of Adsorption Performance. *Polymers* **2017**, *10* (1), 1–19.
650 https://doi.org/10.3390/polym10010025.

651 (63) Liu, W.; Sun, B.; Qiao, J.; Guan, X. Influence of Pyrophosphate on the Generation of
652 Soluble Mn(III) from Reactions Involving Mn Oxides and Mn(VII). *Environ. Sci. Technol.*
653 **2019**, *53* (17), 10227–10235. https://doi.org/10.1021/acs.est.9b03456.

654 (64) Qian, A.; Zhang, W.; Shi, C.; Pan, C.; Giammar, D. E.; Yuan, S.; Zhang, H.; Wang, Z.
655 Geochemical Stability of Dissolved Mn(III) in the Presence of Pyrophosphate as a Model
656 Ligand: Complexation and Disproportionation. *Environ. Sci. Technol.* **2019**, *53* (10), 5768–
657 5777. https://doi.org/10.1021/acs.est.9b00498.

658 (65) Kostka, J. E.; Luther, G. W.; Nealson, K. H. Chemical and Biological Reduction of Mn
659 (III)-Pyrophosphate Complexes: Potential Importance of Dissolved Mn (III) as an
660 Environmental Oxidant. *Geochim. Cosmochim. Acta* **1995**, *59* (5), 885–894.
661 https://doi.org/10.1016/0016-7037(95)00007-0.

(66) Murray, J. W.; Balistrieri, L. S.; Paul, B. The Oxidation State of Manganese in Marine Sediments and Ferromanganese Nodules. *Geochim. Cosmochim. Acta* **1984**, *48* (6), 1237–1247. https://doi.org/10.1016/0016-7037(84)90058-9.

(67) Peña, J.; Kwon, K. D.; Refson, K.; Bargar, J. R.; Sposito, G. Mechanisms of Nickel Sorption by a Bacteriogenic Birnessite. *Geochim. Cosmochim. Acta* **2010**, *74* (11), 3076–3089. https://doi.org/10.1016/j.gca.2010.02.035.

(68) Li, F.; Guo, H.; Zhou, X.; Zhao, K.; Shen, J.; Liu, F.; Wei, C. Impact of Natural Organic Matter on Arsenic Removal by Modified Granular Natural Siderite: Evidence of Ternary Complex Formation by HPSEC-UV-ICP-MS. *Chemosphere* **2017**, *168*, 777–785. https://doi.org/10.1016/j.chemosphere.2016.10.135.

(69) Qin, X.; Liu, F.; Wang, G.; Weng, L. Simultaneous Analysis of Small Organic Acids and Humic Acids Using High Performance Size Exclusion Chromatography. *J. Sep. Sci.* **2012**, *35* (24), 3455–3460. https://doi.org/10.1002/jssc.201200414.

(70) Liu, G.; Cai, Y. Studying Arsenite-Humic Acid Complexation Using Size Exclusion Chromatography-Inductively Coupled Plasma Mass Spectrometry. *J. Hazard. Mater.* **2013**, *262*, 1223–1229. https://doi.org/10.1016/j.jhazmat.2012.05.043.

(71) Elzinga, E. J.; Kustka, A. B. A Mn-54 Radiotracer Study of Mn Isotope Solid−Liquid Exchange during Reductive Transformation of Vernadite (δ-MnO2) by Aqueous Mn(II). *Environ. Sci. Technol.* **2015**, *49*, 4310–4316.

(72) Fakour, H.; Lin, T. F. Experimental Determination and Modeling of Arsenic Complexation with Humic and Fulvic Acids. *J. Hazard. Mater.* **2014**, *279*, 569–578. https://doi.org/10.1016/j.jhazmat.2014.07.039.

(73) Qin, W.; Tan, P.; Song, Y.; Wang, Z.; Nie, J.; Ma, J. Enhanced Transformation of Phenolic Compounds by Manganese(IV) Oxide, Manganese(II) and Permanganate in the Presence of Ligands: The Determination and Role of Mn(III). *Sep. Purif. Technol.* **2021**, *261*. https://doi.org/10.1016/j.seppur.2020.118272.

(74) Tani, Y.; Miyata, N.; Ohashi, M.; Ohnuki, T.; Seyama, H.; Iwahori, K.; Soma, M. Interaction of Inorganic Arsenic with Biogenic Manganese Oxide Produced by a Mn-Oxidizing Fungus, Strain KR21-2. *Environ. Sci. Technol.* **2004**, *38* (24), 6618–6624. https://doi.org/10.1021/es049226i.

(75) Lafferty, B. J.; Ginder-Vogel, M.; Sparks, D. L. Arsenite Oxidation by a Poorly-Crystalline Manganese Oxide. 3. Arsenic and Manganese Desorption. *Environ. Sci. Technol.* **2011**, *45* (21), 9218–9223. https://doi.org/10.1021/es201281u.

(76) Parikh, S. J.; Lafferty, B. J.; Meade, T. G.; Sparks, D. L. Evaluating Environmental Influences on AsIII Oxidation Kinetics by a Poorly Crystalline Mn-Oxide. *Environ. Sci. Technol.* **2010**, *44* (10), 3772–3778. https://doi.org/10.1021/es903408g.

(77) Li, Q.; Xie, L.; Jiang, Y.; Fortner, J. D.; Yu, K.; Liao, P.; Liu, C. Formation and Stability of NOM-Mn(III) Colloids in Aquatic Environments. *Water Res.* **2019**, *149*, 190–201. https://doi.org/10.1016/j.watres.2018.10.094.

(78) Stone, A. T.; Morgan, J. J. Reduction and Dissolution of Manganese(III) and

Manganese(IV) Oxides by Organics. 1. Reaction with Hydroquinone. *Environ. Sci. Technol.* **1984**, *18* (6), 450–456. https://doi.org/10.1021/es00124a011.

(79) Husnain, S. M.; Asim, U.; Yaqub, A.; Shahzad, F.; Abbas, N. Recent Trends of MnO2-Derived Adsorbents for Water Treatment: A Review. *New J. Chem.* **2020**, *44* (16), 6096–6120. https://doi.org/10.1039/c9nj06392g.

708 **Table of Contents/Art:**

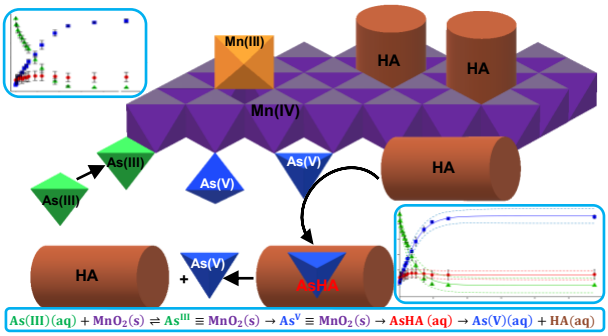


709